Journal of Power Sources 223 (2013) 147–154

Contents lists available at SciVerse ScienceDirect

Journal of Power Sources

journal homepage: www.elsevier.com/locate/jpowsour

Synthesis of large surface area carbon xerogels for electrochemical double layer capacitors

Yun-Min Chang, Cheng-Yeou Wu, Pu-Wei Wu*

Department of Materials Science and Engineering, National Chiao Tung University, 1001 Ta Hsueh Road, Hsin-Chu 300, Taiwan

HIGHLIGHTS

- ► Improved formula for resorcinol–formaldehyde condensation to produce porous carbon structure.
- ► Solvent exchange and carbon dioxide activation to fabricate carbon xerogels with surface area of 3419 $m^2\ g^{-1}$.
- ► Specific capacitance and life time comparable or better than Black Pearl 2000.

ARTICLE INFO

Article history:
Received 4 June 2012
Received in revised form
23 August 2012
Accepted 14 September 2012
Available online 23 September 2012

Keywords:
Carbon xerogels
Electrochemical double layer capacitor
Resorcinol–formaldehyde condensation
Solvent exchange
Carbon dioxide activation

ABSTRACT

A resorcinol–formaldehyde (R–F) condensation reaction catalyzed by acetic acid (C) is employed to prepare carbon xerogels for electrochemical double layer capacitors. The samples are fabricated with an R:F ratio of 1:2 and R:C ratio of 10:1, followed by solvent exchange, pyrolysis, and carbon dioxide activation. The solvent exchange allows negligible structure contraction upon drying, and after pyrolysis and carbon dioxide treatment, we are able to produce porous carbons with a surface area of 3419 $m^2\ g^{-1}$. Image from scanning electron microscope reveals an interconnected foam-like structure and BET confirms the presence of excessive micro- and mesopores. Electrochemical analysis including cyclic voltammetry (CV), current reversal chronopotentiometry (CRC), and impedance spectroscopy are conducted using a titanium cavity electrode so relevant capacitive characteristics and kinetic parameters could be determined. Both CV and CRC results indicate specific capacitances and life time behaviors that are comparable or even better than those of Black Pearl 2000. For example, the specific capacitance is 324.8 F g^{-1} in 0.5 M H_2SO_4 aqueous solution at ±1 A g^{-1} for potential window of 0–1 V. In contrast, sample without carbon dioxide activation displays a similar morphology but its surface area and specific capacitance are reduced considerably to 449 $m^2\ g^{-1}$ and 34.7 F g^{-1}, respectively.

1. Introduction

Supercapacitors have attracted significant attention recently because they demonstrate impressive advantages in power output, energy density, and cycle life, as compared to conventional rechargeable batteries, for the applications in electric vehicles, power tools, and uninterrupted power systems [1–8]. From the standpoint of operation mechanism, there are two types of supercapacitors; electrochemical double layer capacitors (EDLCs) and pseudocapacitors. The EDLCs store charges via ions adsorption/desorption at the interface between the electrode and electrolyte [1–5]. In contrast, the pseudocapacitors entail facile faradaic reactions occurring on the electrode material to store charges in different oxidation states [6–8]. Between them, the pseudocapacitors are able to deliver larger capacitances but with cost premium and relatively finite cycle life. For the EDLCs, the capacitive responses are proportional to the effective surface area available for ions adsorption/desorption so an excessive surface area with a desirable porosity for the electrode material is necessary.

To date, considerable efforts have devoted on carbon-based materials for EDLCs since their rich varieties exhibit a wide range of pore sizes, surface areas, electric conductivities, and surface properties. In literature, carbonaceous materials including active carbons, carbon blacks, glassy carbons, and nanostructured carbons (carbon nanotubes, nanocapsules, nanofibers, gels) have been investigated with various results [9–17]. Among them, the carbon xerogels and aerogels demonstrate unique properties in extremely low density and high porosity [18,19]. The carbon xerogels and aerogels are synthesized via a sol–gel process in which precursors in liquid states are properly mixed, and condense to form

* Corresponding author. Tel.: +886 3 5131227; fax: +886 3 5724727.
E-mail address: ppwu@mail.nctu.edu.tw (P.-W. Wu).

0378-7753/$ – see front matter © 2012 Elsevier B.V. All rights reserved.
http://dx.doi.org/10.1016/j.jpowsour.2012.09.066

continuous colloidal networks, followed by solvent removal and pyrolysis to obtain a porous carbon structure with interconnected channels. One of the sol–gel approaches that has been explored extensively is the polycondensation of resorcinol (R) and formaldehyde (F) [18–20]. According to Elkhatat and Al-Muhtaseb [21], the concentrations for the precursors, catalysts, solvents, and pH play significant roles in determining the resulting morphologies and porosities of the gel structures. In addition, the solvent removal step for the wet gels is rather critical because the drag of surface tension induces contraction of the colloidal networks resulting in substantial reduction in the pore size. So far, many R–F derived porous carbons have been prepared and evaluated for possible applications in EDLCs, catalysis (as a catalyst support), filtration, gas separation, and adsorption [19,22–25].

Previously, many RF-derived xerogels and aerogels have been synthesized and tested for capacitive behaviors [26,27]. The preparation of xerogels involves direct solvent evaporation that engenders notable structural contraction and possible collapse at the extreme case. As a result, after pyrolysis the carbon xerogels typically contain 25% porosity, and reveal a moderate surface area (150–900 $m^2\ g^{-1}$) and small pores (1–10 nm) [28]. In contrast, the carbon aerogels experience a supercritical drying step that sublimates the solvents with negligible shrinkage of carbon networks. After pyrolysis, the carbon aerogels demonstrate a substantially larger surface area and pore volume, and consequently, a larger capacitance [28,29]. Despite those merits, the carbon aerogels are of little commercial interest because the supercritical drying is energy-consuming and not adaptable for production in large quantity. On the other hand, the carbon xerogels suffer from unnecessary structure alteration and hence, their pore size and pore volume are not adequate for EDLC applications. An alternative preparation route to minimize structure contraction during sol–gel transformation is via repeated solvent exchanges that reduce the surface tension of the solvent sequentially in the wet gels [27]. In this way, the solvent with reduced surface tension is able to evaporate slowly rendering a dried gel known as “ambient gel” whose structure closely resembles to that of aerogel. This enables a large number of mesopores and macropores in the carbon skeleton. This ambient gel represents a unique form of xerogels, and could be of potential interest because its desirable surface area and porosity, as well as simple drying process.

It is understood that desirable EDLCs require large surface areas with appropriate pore sizes for facile access of ions from the electrolyte during capacitive charging and discharging. This can be realized by fabricating suitable carbon skeletons followed by a deliberate activation step to remove atomic carbon selectively. In this work, we explore the preparation of RF-derived xerogels in conjunction with solvent exchange and carbon dioxide treatment for surface activation so an excessive surface area and suitable pore size can be obtained. The resulting materials are subjected to electrochemical measurements using a titanium cavity electrode (TCE) to determine their intrinsic capacitive behaviors and relevant kinetic parameters.

2. Experimental

The carbon xerogel was prepared by a condensation reaction between resorcinol and formaldehyde, followed by solvent exchange, pyrolysis, and carbon dioxide activation to render an excessive surface area. First, resorcinol (R) and 37 wt% formaldehyde (F) were properly mixed in a 1:2 M ratio in deionized water (W) under ultrasonication for 10 min at 26 °C. After complete dissolution of resorcinol, 99 wt% acetic acid (C) was added as a catalyst to promote the condensation reaction forming colloids in the mixture. Subsequently, the mixture was sealed in a container at 70 °C for 72 h with constant vibration to allow the transformation from a sol suspension to a wet gel. The wet gel maintained a cylindrical shape of $\pi \times (2.25)^2 \times 4.2\ cm^3$. After gelation, the sample was removed from the oven and washed for 72 h in which 50% of acetone was drained and replaced with fresh acetone every 24 h. Next, the process was repeated again for another 72 h with cyclohexane. These solvent exchange steps were conducted at 26 °C so the surface tension for the liquid phase was reduced sequentially to avoid structural contraction for the solid phase upon solvent evaporation. At this stage, the sample maintained its size without noticeable shrinkage. Afterward, the sample was dried at 26 °C for 24 h to evaporate remaining cyclohexane, leaving a free-standing dark orange gel in size of $\pi \times (2.05)^2 \times 4.1\ cm^3$. This corresponded to a volume shrinkage of 19%. In contrast, an as-prepared sample dried directly under ambient condition without solvent exchange reduced its size to $\pi \times (1.69)^2 \times 3.4\ cm^3$, which amounted to 54% volume reduction. Finally, the sample was placed in a tube furnace for two-stage heat treatments. The first stage was performed in argon atmosphere (99.99%) at 950 °C for 1 h to decompose organic residues (pyrolysis reaction) where the dark orange sample shrunk significantly becoming a black porous carbon. The heating profile included 10 °C min^{-1} for 25–600 °C, 6 °C min^{-1} for 600–900 °C, and 1 °C min^{-1} for 900–950 °C. In the second stage, at 950 °C the argon was purged quickly via vacuum pump (1 min) and 99.99% carbon dioxide was introduced for 3 h to activate the surface of the porous carbon. Afterwards, the carbon dioxide was again vacuum-pumped and the tube furnace was refilled with argon to allow slow cooling to room temperature for roughly 12 h. By adjusting precursor and catalyst concentration, we were able to prepare xerogels with various porosities and surface areas. The resulting samples were designated as GA, GB, and GC, respectively. The exact amounts for the precursors, catalyst, deionized water, as well as ratios for the R/C and R/W are listed in Table 1. In order to distinguish the effect of carbon dioxide activation, we also carried out identical processing steps except the carbon dioxide activation was replaced with argon treatment for another 3 h (labeled as GD as a reference sample).

The morphologies for the xerogels after pyrolysis and carbon dioxide activation were observed by an SEM (JEOL JSM-6500F). Surface area was determined by Quantachrome NOVA-1000A where a density functional theory (DFT) program was employed to estimate relevant parameters in pore size and pore distribution. The DFT is a mathematic approach to describe gas adsorption behaviors over a wide range of pressures and temperatures after taking into account of population density, energy, and equilibrium between the adsorbing molecules and substrate [30].

For electrochemical analysis to determine the double layer capacitance, a three-electrode cell was used in which a J-shaped TCE, with 2 mm in diameter and 200 mm in length, was adopted as the working electrode. The bottom of the TCE contained a cylindrical cavity with 1 mm in diameter and 1 mm in depth for sample

Table 1
Precursors and catalyst used for the synthesis of carbon xerogels.

		GA	GB	GC	GD
Precursors	R: resorcinol (g)	9.25	14.75	14.75	14.75
	F: formaldehyde (g)	5.05	8.04	8.04	8.04
Catalyst	C: acetic acid (μL)	965	1533	766.5	766.5
Solvent	W: deionized water (g)	50	50	50	50
	R:F	1:2	1:2	1:2	1:2
Molar ratio	R:C	5:1	5:1	10:1	10:1
	R:W	1:5.4	1:3.4	1:3.4	1:3.4
	Burn-off[a] (wt%)	95.3	95.3	96.4	88.3

[a] Total weight loss of carbon xerogels after 950 °C pyrolysis and carbon dioxide activation.

loading. The sample was placed on a glass sheet and pressed into fine powders so they filled compactly into the bottom cavity. The exact weight was measured by a microbalance with an accuracy of 10 μg, and in our cases, the sample weights were between 2 and 3 mg. Details on the TCE and its testing results on commercially available carbon blacks have been reported earlier [31]. Pt foil (2×5 cm^2) and Ag/AgCl were used as the counter and reference electrodes, respectively. Values for the double layer capacitance were determined via cyclic voltammetry (CV) and current reversal chronopotentiometry (CRC) in 0.5 M H_2SO_4 aqueous solution at 26 °C using a Solartron SI1287 potentiostat and 1255B frequency response analyzer. The CV profiles were recorded at scan rates of 5, 10, 20, and 50 mV s^{-1}, in potential windows of 0–0.6, 0–0.8, and 0–1 V, respectively. The CRC measurements were carried out at ±1 A g^{-1} in a potential window of 0–1 V. In life time evaluation, the sample was subjected to repeated CRC scans at ±1 A g^{-1} in a potential window of 0–1 V. Impedance spectra were obtained at the open circuit voltage with a sinusoidal signal of 10 mV for frequencies between 0.1 and 20 kHz. The resulting spectra were fitted by a ZView software to retrieve relevant electrochemical parameters.

3. Results and discussion

Previously, in the preparation of R–F-derived carbon aerogels, the R/C ratios were kept between 50 and 1500, and a basic catalyst such as sodium carbonate was used [21]. It is because a high R/C ratio enables the formation of large colloidal particles with limited contacts among them, and a base catalyst promotes a wider pore size distributions [20,21]. However, in their formula the concentration for the catalyst is extremely low and it becomes rather difficult to initiate condensation reaction homogeneously. Therefore, we rationalize that a lower R/C ratio of 5 or 10 might be beneficial because the concentrated precursors engender an intimate structure with relatively narrower pore size distribution. In addition, we select an acidic catalyst because Al-Muhtaseb et al. and Elkhatat et al. observed that in an acidic solution, the condensation reaction took less time to complete and finer interconnected mesopores were produced afterwards [20,21].

Representative SEM images for GA, GB, GC, and GD are provided in Fig. 1. Sample GA (shown in Fig. 1(a) and its inset) revealed uniform spherical carbons with diameter in 7–10 μm. These spherical carbons were contacting each other in a string-of-pearls pattern. This morphology was expected because the sample was synthesized with relatively lower precursor concentrations so the condensation reaction took place slowly forming larger primary particles. Similar behaviors were observed by Scherdei et al. where they observed the formation of spherical particles at lower precursor concentrations [32]. In sample GB exhibited in Fig. 1(b), once the precursor concentrations were increased (while the R/C ratio was kept at 5:1), we observed many small irregularly-shaped carbon particles (50–500 nm in size) connecting to each other. It is realized that during sol–gel transformation, a higher precursor concentration often leads to a faster condensation rate and stronger cross-linking among primary particles. As a result, sample GB demonstrated a foam-like microstructure with mostly smaller primary carbon particles as compared to those of sample GA. Fig. 1(c) displays the morphology for sample GC, where a reduced catalyst amount was used while the precursor concentrations were identical to those of sample GB. Similar to that of Fig. 1(b), there appeared a foam-like microstructure with primary carbon particles in 50–100 nm size. However, at a higher magnification, sample GC revealed larger internal pores and even moderate sintering among primary carbon particles. We understood that due to a reduced catalyst loading, there were fewer nucleation sites for the sol–gel transformation so the resulting cross-linking became less pronounced. Morphology for sample GD is shown in Fig. 1(d). Since the only difference between sample GC and GD was the treatment for carbon dioxide activation, we realized that their morphologies to be quite similar as the carbon dioxide etching effect was

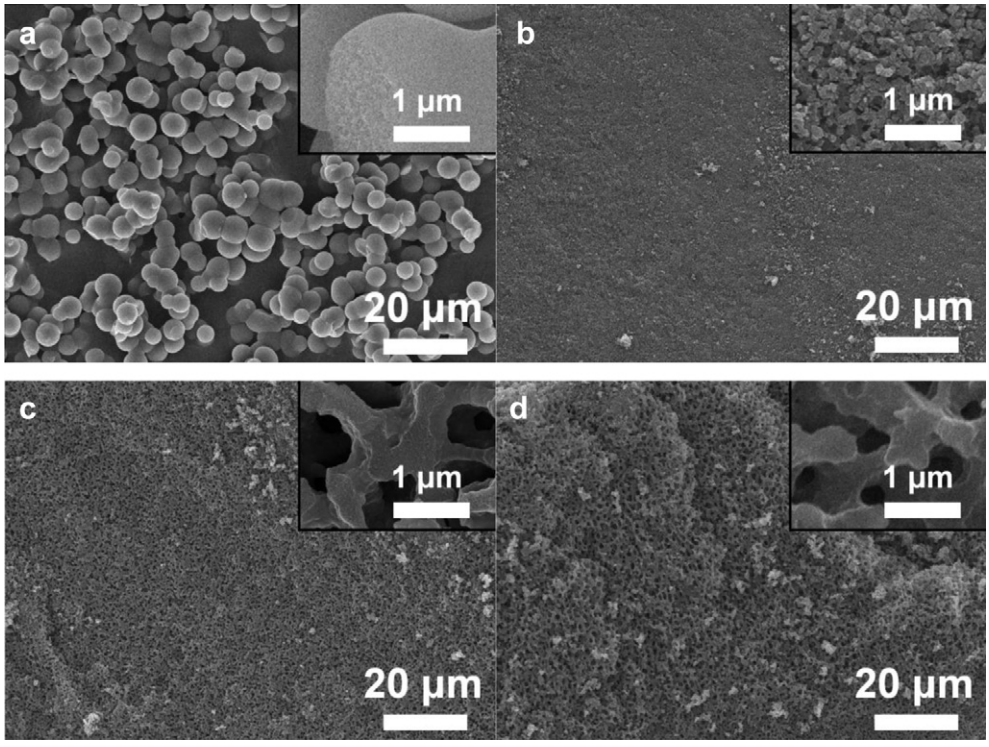

Fig. 1. SEM images for sample (a) GA, (b) GB, (b) GC, and (d) GD.

expected to produce micropores on the carbon surface and those micropores were not readily discernible in SEM observations.

These carbon xerogels are known to possess a variety of pores classified as microspores (<2 nm), mesopores (2–50 nm), and macrospores (>50 nm). Their relative amounts could be estimated by nitrogen adsorption and desorption isotherms, shown in Fig. 2. Interestingly, sample GA, GB, and GC demonstrated a type I behavior, indicating the predominant presence of micropores. Relevant pore properties including BET surface area (S_{BET}), micropore surface area (S_{Micro}), external surface area (S_{Ext}), average pore diameter, micropore volume (V_{Micro}), and total pore volume (V_{Pore}) are provided in Table 2. Despite their notable difference in SEM morphology, sample GA and GB exhibited micropore volumes that were rather close, implying that the R/C ratio and carbon dioxide activation were directly responsible for micropore formation. Remarkably, at identical R/C ratio of 10, sample GC revealed four times larger micropore volume over that of sample GD. Moreover, the external surface area for sample GC was increased considerably as well. It is noted that the external surface area represents the sum of macropores and mesopores. From Fig. 1, the morphologies for sample GC and sample GD were quite similar, and hence their macropore volumes were likely to be close. Therefore, the recorded large external surface area for sample GC was attributed to the formation of abundant mesopores and micropores during carbon dioxide activation. This can be confirmed by the burn-off ratio listed in Table 1. With carbon dioxide activation, the samples suffered from weight loss of 95–96%. In contrast, without carbon dioxide activation, sample GD retained 11.7% weight after pyrolysis. Our experimental results provide definitive evidences for carbon dioxide activation that effectively etches the carbon surface, resulting in the presence of excess micropores and mesopores. The surface area for sample GC was estimated at 3419 $m^2\ g^{-1}$, a value that is significantly larger than typical high surface area carbons like activated carbons or Black Pearl 2000 (BP2000).

In previous studies of RF-derived samples, the largest surface area reported was 3125 $m^2\ g^{-1}$ from a carbon aerogel [33]. In our carbon xerogels we were able to exceed that value by combining improved formula, solvent exchange, and carbon dioxide activation simultaneously. It is noted that by employing a basic catalyst, solvent exchange, and carbon dioxide activation (5% CO_2–95% N_2), Lin and Ritter obtained carbon xerogels with surface areas ≦1600 $m^2\ g^{-1}$ [34]. In contrast, our sample of 3125 $m^2\ g^{-1}$ was catalyzed by acetic acid and the carbon dioxide activation was conducted in 99.99% CO_2 atmosphere. Despite the acidic catalyst is known to promote condensation reaction in RF transformation, the predominant catalyst reported in literature is basic one such as sodium carbonate. To our knowledge, the acetic acid was used once by Brandt et al. to prepare carbon aerogels free of metallic impurities as opposed to those using sodium carbonate [35]. They reported that the pore and particle size can be adjusted to a wide range contingent on the ratios of precursors to acetic acid, and the connectivity of primary particles can be exceptionally high so a fine structure can be obtained. In our case, we surmised that a synergistic effect was occurring between our formula and processing conditions rendering a desirable porous structure which was susceptible to carbon dioxide etching. This is reflected by the intense weight loss after pyrolysis and carbon dioxide activation (88–96%) as compared to that of conventional RF-derived xerogel (50–60%). As a result, our samples revealed excessive surface areas.

Table 2
Relevant parameters for the pore properties determined by nitrogen adsorption and desorption isotherms from GA, GB, GC, and GD, respectively.

	GA	GB	GC	GD
V_{Pore} ($cm^3\ g^{-1}$)	0.99	0.86	1.36	0.23
V_{Micro} ($cm^3\ g^{-1}$)	0.42	0.40	0.76	0.18
S_{BET}[a] ($m^2\ g^{-1}$)	2293.9	2016.6	3418.6	449.1
S_{Micro} ($m^2\ g^{-1}$)	1009	928.8	1987.4	338.4
S_{Ext}[b] ($m^2\ g^{-1}$)	1284.9	1087.7	1431.2	110.7
D_p (Å)	13.8	12.2	18.5	11.1
S_{Ext} ratio[c] (%)	56	53.9	40.9	24.7

[a] $S_{BET} = S_{Micro} + S_{Ext}$.
[b] S_{Ext} is the surface area including mesopores and macropores.
[c] S_{Ext} ratio $= S_{Ext}/S_{BET}$.

In general, the capacitance value for an EDLC is contingent on the electrode fabrication process which affects the resulting composition and structure, as well as measurement techniques involved. Conventional porous composite electrodes and thin film electrodes require certain amount of active materials to mix with binders and conductive additives. Hence, the determination of intrinsic capacitive responses for a potential EDLC material becomes a challenge. Since both binder and conductive additive are not used in TCE analysis, and only a minute amount of active material is necessary, the intrinsic capacitive behaviors can be accurately obtained as established by our earlier work [31]. Fig. 3

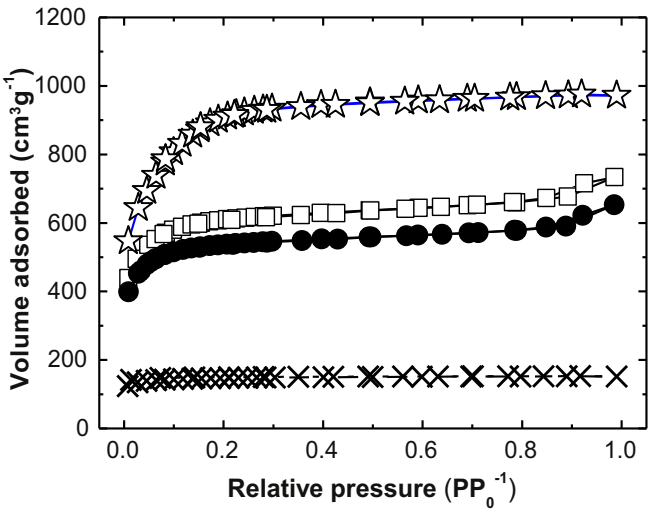

Fig. 2. N_2 adsorption/desorption isotherms of sample GA (□), GB (●), GC (☆), and GD (×).

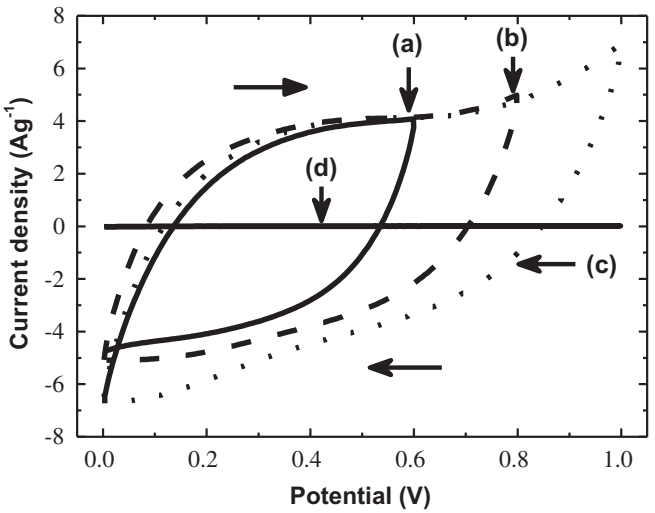

Fig. 3. CV profiles at 20 mV s^{-1} from sample GC in potential windows of (a) 0–0.6 V, (b) 0–0.8 V, (c) 0–1 V, and (d) empty TCE of 0–1 V, respectively.

demonstrates representative CV profiles for sample GC at potential windows of 0–0.6, 0–0.8, and 0–1 V, respectively, along with the response from an empty TCE. As shown, the TCE itself revealed negligible currents in both forward and backward scans. In contrast, the carbon xerogels exhibited quasi-rectangular responses typical of EDLCs [36]. At voltage approaching 1 V, there appeared moderate electrolysis which engendered an apparent current rise. Notably, the presence of functional groups on the carbon xerogels was rather subdued as additional redox peaks were not observed in 0.2–0.6 V. It is known that the specific capacitance could be estimated from the CV profiles by the equation listed below,

$$C_s = \frac{Q}{w\Delta E} = \frac{\int i_c dt}{w\Delta E} \quad [1]$$

where C_S, Q, w, ΔE, and ic are the specific capacitance (F g^{-1}), coulombs of discharge, sample weight, CV potential window, and cathodic current density, respectively. Table 3 lists the specific capacitance for the carbon xerogels at various potential windows along with commercially available carbon blacks such as Vulcan XC72R (XC72R), BP2000, and Active Carbon (AC1100). The specific capacitances for those commercial carbon blacks were determined by a TCE in identical testing conditions, and their values were reported in our previous work [31].

Among commercial carbon blacks, the BP2000 is known to possess a large surface area due to its fine particle size and consequently, its capacitance is considerably larger than that of XC72R (130.3 vs. 25.7 F g^{-1}). Remarkably, the carbon xerogels of GB and GC demonstrated even larger specific capacitances, reaching values of 150.4 and 209.9 F g^{-1}, respectively. These values, to our knowledge, are comparable to the capacitances derived from other large surface area nanostructured carbons reported in literature [37–41]. For example, Weng et al. fabricated active carbons with a surface area of 2860 m^2 g^{-1} and obtained a capacitance of 130 F g^{-1} [37]. Similar results were reported by Rufford et al. where active carbons of 1788 and 2019 m^2 g^{-1} were synthesized and their capacitances were recorded at 300 and 368 F g^{-1}, respectively [38,39]. From Table 1, sample GD was produced with identical formulation like sample GC but the carbon dioxide activation step was replaced with argon heat treatment. Without the carbon dioxide etching effect, sample GD revealed a substantially reduced micropore volume and as a result, its specific capacitance was merely 38.3 F g^{-1}.

It is understood that the CV profiles for a double layer capacitor are affected by the scan rate imposed during CV measurements. The relation for a capacitive current from a double layer capacitor is listed below,

$$i_c = vC_d\left[1 - \exp\left(-\frac{t}{R_sC_d}\right)\right] \quad [2]$$

where ic is defined previously, v is the scan rate, Rs represents the electrolyte resistance, t is the time, and C_d is the capacitance (F g^{-1}). Hence, the current rises quickly and reaches a plateau in a short time for a true capacitor. In addition, an increasing scan rate engenders a larger current plateau. Fig. 4 displays representative CV profiles for sample GC at various scan rates in a potential window of 0–1 V. The CV profiles demonstrated rectangular shapes at scan rates of 5 and 10 mV s^{-1}, which were expected for a typical double layer capacitor [42]. Apparently, once the scan rate was increased to 20 mV s^{-1} and above, the resulting CV curves became moderately distorted. This distortion was attributed to the compromised diffusion within the porous structure that rendered a progressively slower capacitance upon faster scan rate [31]. The specific capacitance is also a function of CV scans since at a sufficiently fast scan rate, some micropores become inaccessible due to diffusion limitation, and thus cease to contribute to the capacitive current. Hence, the largest specific capacitance is always recorded at the lowest scan rate where ions adsorption and desorption are possible in available free surface and internal pores. Table 4 provides the specific capacitance at different scan rates for the carbon xerogels and commercial carbon blacks. For the carbon xerogels except sample GA, they exhibited capacitance retention characteristics similar to those of XC72, BP2000, and AC1100. We can thus reasonably assumed that the carbon xerogels contained pores that were properly sized so access by ions was compromised moderately at fast scan rate.

Fig. 5 provides the CRC responses at ±1 A g^{-1} for the carbon xerogels. It is established that the specific capacitance can be estimated by following equation,

$$C_s = \frac{\dfrac{i_c}{(w \times |dE|)}}{dt} \approx \frac{Q}{w \times \Delta E} \quad [3]$$

where C_S, w, ic, and Q are defined previously, and dE/dT is the slope for discharging curve. In addition, during current reversal, there is a sudden voltage drop (iR loss) whose magnitude is proportional to the electrical resistance of carbon xerogels, TCE, and electrolyte. Values for the specific capacitance and iR loss are listed in Table 5. As listed, sample GD demonstrated the lowest voltage drop, suggesting its smallest electrical resistance. This might be attributed to its intimate interconnected structure and surface integrity. On the other hand, sample GA revealed the largest voltage drop which was likely caused by the finite contact areas among primary carbon particles that circumvented electron transports (see Fig. 1(a)). In

Table 3
Values of specific capacitance (F g^{-1}) calculated from CV profiles in various potential windows at 20 mV s^{-1} scan rate.

	GA	GB	GC	GD	XC72[a]	BP2000[a]	AC1100[a]
0–0.6 V	55.8	98	168.4	31	16.7	78	75
0–0.8 V	69.3	115.2	183.4	33	18.7	94	80.8
0–1 V	84.5	150.4	209.9	38.3	25.7	130.3	88

[a] These values were reported in reference [31].

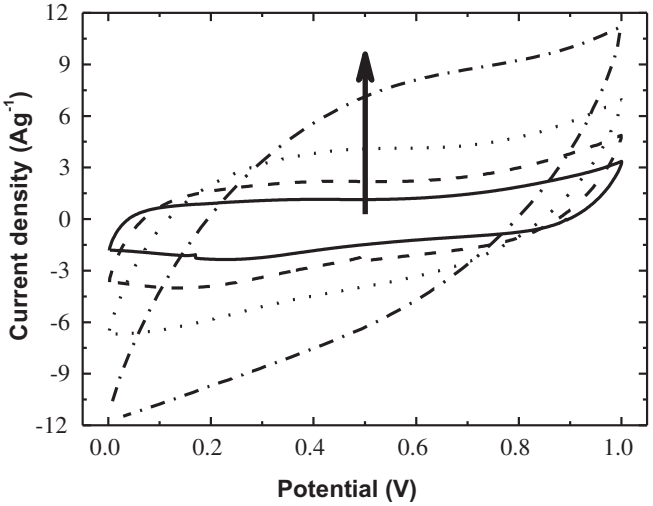

Fig. 4. CV profiles for sample GC in potential window of 0–1 V at scan rates of 5, 10, 20, and 50 mV s^{-1}, respectively.

Table 4
Values of specific capacitance (F g^{-1}) calculated from CV profiles at various scan rates in potential window of 0–1 V.

mV s^{-1}	GA	GB	GC	GD	XC72[a]	BP2000[a]	AC1100[a]
5 (a)	193.7	214.9	312.3	56.9	32.03	169.76	128.48
10	132.4	183.1	266.2	47.2	29.52	152.97	111.19
20	84.5	150.4	209.9	38.3	25.68	130.32	88
50 (b)	38.6	122.6	132.6	27.3	23.28	95.51	51.28
(b/a) (%)	19.9	57.1	42.5	48.8	72.68	56.26	39.91

[a] These values were reported in reference [31].

Table 5
Relevant parameters determined from the CRC measurements at ±1 A g^{-1} in potential window of 0–1 V.

	GA	GB	GC	GD
Q (C)	236.3	269.2	418.6	39.60
E^+ (V)	1.00	1.00	1.00	1.00
E^- (V)	0.736	0.869	0.935	0.944
iR drop (mV)	264	131	65	56
C_S (F g^{-1})	213.2	229.4	324.8	34.7

addition, all carbon xerogels except GD demonstrated specific capacitances larger than 200 F g^{-1}, indicating that accessible surface area, as well as suitable microspores and mesopores structure were produced after carbon dioxide activation.

It is noted that the CRC method always leads to a higher specific capacitance as opposed to that of CV scans. It is because the CRC method is conducted at a fixed potential window with a constant current density and therefore, the process allows sufficient time for ion adsorption and desorption. In contrast, the capacitance determined from the CV scans is caused by a varying current so the kinetics for ion diffusion in the porous structure becomes a limiting factor. In principle, the capacitance obtained at slow scan rate during CV scans is likely to approach that of CRC method. In our measurements, indeed, the capacitance from the CRC method at 1 A g^{-1} was rather close to the capacitance from the CV profile with a scan rate of 5 mV s^{-1}.

To evaluate life time performance for the carbon xerogels, we carried out repeated CRC experiments between 0 and 1 V at ±1 A g^{-1}. The resulting capacitance variation over 3000 cycles are shown in Fig. 6, along with that of BP2000 for comparison purpose. In life time testing, it was found that the capacitances became smaller with increasing cycles, a fact that was possibly associated with detachment of individual carbon particles upon prolonged cycling. We surmised that without binder, electrolyte inundation in the TCE cavity inevitably affected packing density and local environments of the carbon particles. As a result, the amount of carbon particles responsible for capacitive responses was decreasing with time. This undesirable effect was most severe in sample GA (with a capacity loss of 63%) since from SEM image there was limited contact between carbon particles so poor electrical conductivity and packing density were not unexpected. In contrast, sample GB revealed impressive capacitance retention with a moderate capacity loss of 13%. In contrast, sample GC showed a capacitance loss of 27% despite its *iR* loss was the least from Table 5. Nevertheless, its value was still significantly better than 41% of BP2000. From Fig. 6, we concluded that except sample GA, the carbon xerogels retained reasonable EDLCs behaviors comparable or even better than that of BP2000.

Impedance analysis is a powerful technique to examine the interfacial phenomenon taking place on the carbon xerogels during capacitive responses. Our impedance spectra were obtained at the open circuit voltage and their values were 0.4119, 0.3327, and 0.3458 V (vs. Ag/AgCl) for GA, GB, and GC, respectively. Fig. 7(a) demonstrates the Nyquist plots over the entire frequency regime. Apparently, the impedance spectra were consisted of a semi-circle at high frequency and a Warburg diffusion at low frequency. The enlarged spectra at high frequency regime is shown in Fig. 7(b) and the equilivent circuit model used to fit the impedance spectra is provided in Fig. 7(c). As shown, the equilivent circuit includes elements of R_s (ohmic resistance from electrolyte, carbon particles, and TCE), R_{CT} (resistance from faradaic charge transfer reaction), CPE_p (constant phase element for faradaic charge transfer reaction), W (Warburg impedance), and CPE_{EDL} (constant phase element for electrochemical double layer). For both CPE_p and CPE_{EDL}, they can be derived from following equation [43]:

$$Z = \frac{I}{T(j\omega)^{\alpha}} \quad [4]$$

where Z, T, j, ω, and α are impedance, capacitance of associated element, imaginary unit, angular frequency ($\omega = 2\pi f$) of the AC signal, and a dimensionless parameter for fitting purpose ($\alpha = 0$ for a pure resistor and $\alpha = 1$ for an ideal parallel plate capacitor). In

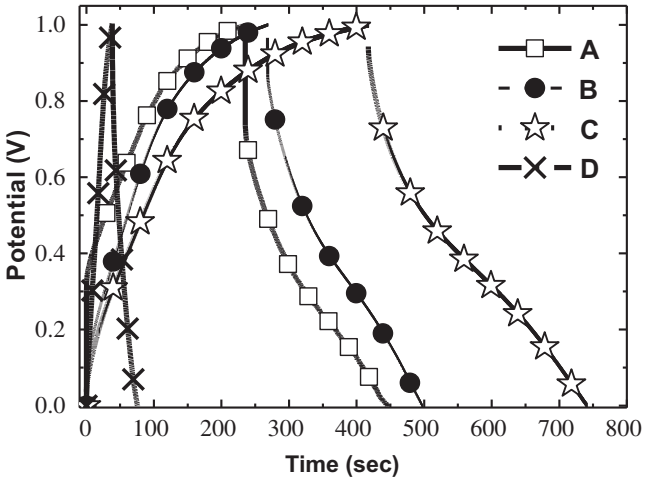

Fig. 5. CRC curves at ±1 A g^{-1} in potential window of 0–1 V for sample GA, GB, GC, and GD, respectively.

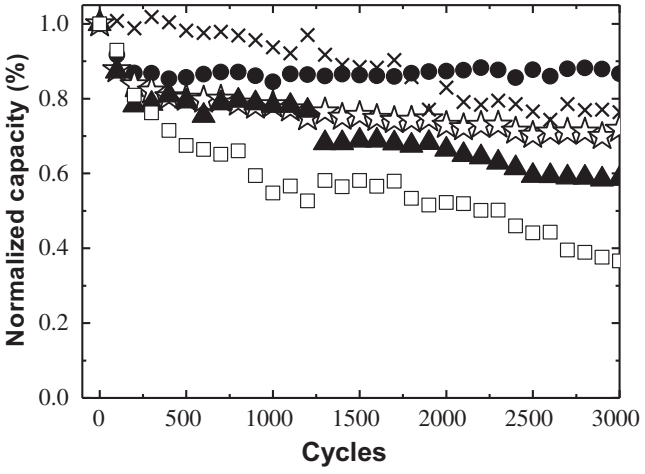

Fig. 6. Variation of specific capacitance for sample GA(□), GB(●), GC(☆), GD(×), and BP2000 (▲) obtained from CRC measurements in potential window of 0–1 V at ±1 A g^{-1} for 3000 cycles.

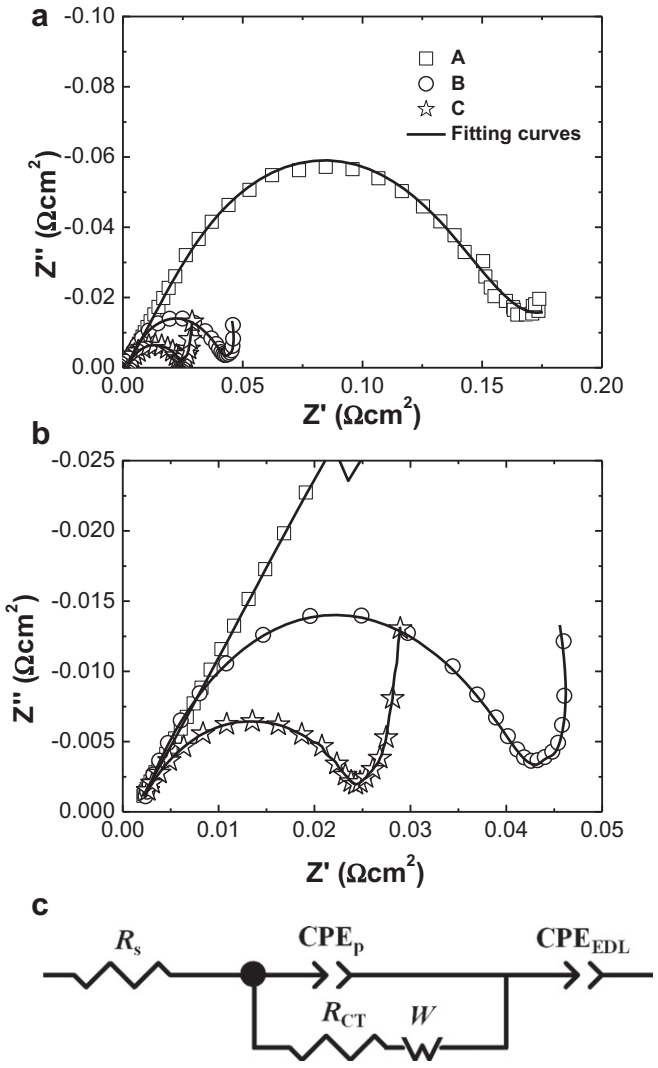

Fig. 7. (a) Nyquist plots for sample GA, GB, and GC at the open circuit voltage in frequency range of 0.1–20 kHz, as well as (b) the enlarged spectra at high frequency regime. (c) The equivalent circuit model used to fit the impedance spectra.

practice, the α is between 0 and 1, and its exact value reflects the porous nature of the active material [44].

Table 6 presents fitting results with relevant parameters clearly identified. As listed, the R_s values were rather subdued confirming the conductive nature for the carbon xerogels. The CPE_p–T, W–T, and CPE_{EDL}–T indicate the capacitive components for CPE_p, Warburg impedance, and CPE_{EDL}, respectively. Among these samples, the α values for CPE_p were consistently below 1, which was expected for a porous electrode. In addition, the α values of Warburg impedance for sample GB and GC were under 1, a fact attributed to the limited diffusion in porous carbons. For sample GA, its α-value of Warburg impedance was undetermined because the Warburg diffusion occurring at the low frequency regime was not clearly defined. It is possible that a lower frequency AC signal is necessary to better distinguish the diffusion effect. As for the CPE_{EDL}, interestingly, sample GC revealed a α-value of 1, suggesting its response was close to an ideal capacitor.

Table 6
Parameters from fitting impedance spectra obtained at the open circuit voltage.

		GA	GB	GC
R_s (Ω g^{-1})		0.00115	0.00181	0.00151
CPE_p	T (F g^{-1})	1.113	0.228	0.281
	α	0.553	0.707	0.642
R_{CT} (Ω g^{-1})		0.0954	0.0339	0.0215
W	R (Ω g^{-1})	–	0.0019204	0.00462
	T (F g^{-1})	–	0.69332	0.839
	α	–	0.741	0.417
CPE_{EDL}	T (F g^{-1})	77.230	117.300	130.300
	α	0.428	0.552	1.000

4. Conclusions

We synthesized carbon xerogels via a condensation reaction of resorcinol and formaldehyde, followed by solvent exchange, pyrolysis, and carbon dioxide activation. The carbon xerogels experienced negligible structural contraction during solvent removal and as a result, demonstrated excessive surface area with a large number of micropores and mesopores. By selecting suitable combination of precursors and acidic catalyst, we were able to produce a porous carbon structure whose surface area reached as high as 3418 m^2 g^{-1}. Image from SEM confirmed its foam-like morphology with moderate sintering among primary carbon particles. CV scans and CRC methods indicated specific capacitances and life time behaviors that were comparable or even better than those of BP2000 in identical testing conditions. In contrast, without carbon dioxide activation, the carbon xerogels displayed a similar morphology but its surface area was reduced considerably to 449 m^2 g^{-1}. Due to lack of sufficient micropores and mesopores, the resulting specific capacitance and life time behavior were substantially inferior to samples with carbon dioxide activation.

Acknowledgements

Financial supports from National Science Council (NSC100-2221-E009-075-MY3) and Taiwan Power Company are greatly appreciated.

References

[1] B.E. Conway, Electrochemical Supercapacitors, Kluwer–Plenum Press, New York, 1999.
[2] P. Kossyrev, J. Power Sources 201 (2012) 347–352.
[3] M.C. Liu, L.B. Kong, P. Zhang, Y.C. Luo, L. Kang, Electrochim. Acta 60 (2012) 443–448.
[4] M. Lazzari, M. Mastragostino, A.G. Pandolfo, V. Ruiz, F. Soavi, J. Electrochem. Soc. 158 (2011) A22–A25.
[5] M. Winter, R.J. Brodd, Chem. Rev. 104 (2004) 4245–4269.
[6] C.J. Hung, J.H. Hung, P. Lin, T.Y. Tseng, J. Electrochem. Soc. 158 (2011) A942–A947.
[7] K.H. Chang, C.C. Hu, C.M. Huang, Y.L. Liu, C.I. Chang, J. Power Sources 196 (2011) 2387–2392.
[8] C.C. Hu, K.H. Chang, M.C. Lin, Y.T. Wu, Nano Lett. 6 (2006) 2690–2695.
[9] Q. Li, F. Liu, L. Zhang, B.J. Nelson, S. Zhang, C. Ma, X. Tao, J. Cheng, X. Zhang, J. Power Sources 207 (2012) 199–204.
[10] J. Ahmed, H.J. Kim, S. Kim, J. Electrochem. Soc. 159 (2012) B497–B501.
[11] B. Haghighi, M.A. Tabrizi, Electrochim. Acta 56 (2011) 10101–10106.
[12] I.G. Casella, D.A. Di Fonzo, Electrochim. Acta 56 (2011) 7536–7540.
[13] E.L.K. Chng, M. Pumera, Electrochem. Commun. 13 (2011) 781–784.
[14] Y.M. Chang, Y.C. Hsieh, P.W. Wu, Diamond Relat. Mater. 18 (2009) 501–504.
[15] M.M. Hasani-Sadrabadi, I. Shabani, M. Soleimani, H. Moaddel, J. Power Sources 196 (2011) 4599–4603.
[16] L. Zou, R. Lv, F. Kang, L. Gan, W. Shen, J. Power Sources 184 (2008) 566–569.
[17] J. Rooke, C.d.M. Passos, M. Chatenet, R. Sescousse, T. Budtova, S. Berthon-Fabry, R. Mosdale, F. Maillard, J. Electrochem. Soc. 158 (2011) B779–B789.
[18] R.W. Pekala, US patent No. 4873218 (1989).
[19] B. Liu, S. Creager, J. Power Sources 195 (2010) 1812–1820.
[20] S.A. Al-Muhtaseb, J.A. Ritter, Adv. Mater. 15 (2003) 101–114.
[21] A.M. Elkhatat, S.A. Al-Muhtaseb, Adv. Mater. 23 (2011) 2887–2903.
[22] C. Arbizzani, S. Beninati, E. Manferrari, F. Soavi, M. Mastragostino, J. Power Sources 161 (2006) 826–830.
[23] A.K. Meena, G.K. Mishra, P.K. Rai, C. Rajagopal, P.N. Nagar, J. Hazard. Mater. 122 (2005) 161–170.
[24] T. Yamamoto, A. Endo, T. Ohmori, M. Nakaiwa, Carbon 42 (2004) 1671–1676.

[25] H.Y. Tian, C.E. Buckley, M. Paskevicius, D.A. Sheppard, S.B. Wang, C.J. Webb, E.M. Gray, Int. J. Hydrogen Energy 36 (2011) 10855–10860.
[26] M. Inagaki, H. Konno, O. Tanaike, J. Power Sources 195 (2010) 7880–7903.
[27] M. Lazzari, F. Soavi, M. Mastragostino, J. Power Sources 178 (2008) 490–496.
[28] H.T. Jespersen, K. Allermann, I. Schneider, K. Schaumburg, US patent No. 20100269731 (2010).
[29] B. Fang, L. Binder, J. Power Sources 163 (2006) 616–622.
[30] P.A. Webb, C. Orr, Analytic Methods in Fine Particle Technology, Micromeritics Instrument, Georgia, 1997.
[31] C.Y. Wu, P.W. Wu, P. Lin, J. Power Sources 195 (2010) 5122–5129.
[32] R. Brandt, J. Fricke, J. Non-Cryst. Solids 350 (2004) 131–135.
[33] T.F. Baumann, M.A. Worsley, T.Y.J. Han, J.H. Satcher Jr., J. Non-Cryst. Solids 354 (2008) 3513–3515.
[34] C. Lin, J.A. Ritter, Carbon 38 (2000) 849–861.
[35] R. Brandt, R. Petricevic, H. Pröbstle, J. Fricke, J. Porous Mater. 10 (2004) 171–178.
[36] B.E. Conway, W.G. Pell, J. Power Sources 105 (2002) 169–181.
[37] T.C. Weng, H. Teng, J. Electrochem. Soc. 148 (2001) A368–A373.
[38] T.E. Rufford, D. Hulicova-Jurcakova, K. Khosla, Z. Zhu, G.Q. Lu, J. Power Sources 195 (2010) 912–918.
[39] T.E. Rufford, D. Hulicova-Jurcakova, Z. Zhu, G.Q. Lu, Electrochem. Commun. 10 (2008) 1594–1597.
[40] Y. Zhu, H. Hu, W. Li, X. Zhang, Carbon 45 (2007) 160–165.
[41] J.S. Ye, X. Liu, H.F. Cui, W.D. Zhang, F.S. Sheu, T.M. Lim, Electrochem. Commun. 7 (2005) 249–255.
[42] J. Wang, M. Chen, C. Wang, J. Wang, J. Zheng, J. Power Sources 196 (2011) 550–558.
[43] X. Liu, L. Juan, L. Zhan, L. Tang, Y. Wang, W. Qiao, J. Electroanal. Chem. 642 (2010) 75–81.
[44] H.K. Song, H.Y. Hwang, K.H. Lee, L.H. Dao, Electrochim. Acta 45 (2000) 2241–2257.